ELSEVIER

Journal of Alloys and Compounds 293–295 (1999) 756–761

Journal of ALLOYS AND COMPOUNDS

Effect of rapid solidification process on the alloy structure and electrode performance of $Zr(Ni_{0.55}V_{0.1}Mn_{0.3}Cr_{0.55})_{2.1}$

Kangying Shu[a,*], Yongquan Lei[a], Xiaoguang Yang[a], Ganfu Lin[a], Qidong Wang[a], Guanglie Lü[b], Lingshen Chen[b]

[a]*Department of Materials Science and Engineering, Zhejiang University, Hangzhou, 310027, PR China*
[b]*Center Laboratory, Zhejiang University, Hangzhou, 310028 PR China*

Abstract

The crystal structure, microstructure, phase abundance and electrochemical properties of $Zr(Ni_{0.55}V_{0.1}Mn_{0.3}Cr_{0.55})_{2.1}$ prepared by the melt spinning method were studied. The results show that the discharge capacity decreases, the number of activation cycles increases and the electrochemical cycle life prolongs while the cooling rate of the hydrogen storage alloy ribbon increases. We discovered a new microstructure, microcrystalline C14 Laves phase in the experiment. The amount of the microcrystalline C14 Laves phase increased with the cooling rate of alloy ribbons. A more detailed study also showed that the electrochemical properties changed with phase abundance (C14 or C15) of alloys prepared at different cooling rates. The phase abundance change of microcrystalline C14 or C15 Laves phases resulted in a discharge capacity change. The increase in phase abundance of the microcrystalline C14 Laves phase had a negative effect on the discharge capacity and activation process, and a positive effect on the cyclic life of the melt spun alloys.

Keywords: Hydride electrode; Melt spinning method; High cooling rate; Microcrystalline C14 Laves phase

1. Introduction

Ni–MH secondary batteries have become a new type power source and used widely in portable computer, wireless telephone, and electric toys etc. due to their good comprehensive electrochemical properties. Negative electrode material of Ni–MH secondary batteries has been mainly AB_5-type mischmetal hydrogen storage alloys until now. The main drawbacks of AB_5 type hydrogen storage alloys are their low capacity and poor cyclic endurance. Compared with AB_5 type hydride electrode alloys, Zr-based AB_2 type Laves phase hydrogen storage alloys, owing to their higher theoretic electrochemical capacity, are promising new electrode alloys which have been widely investigated all over the world.

Rapid solidification as an advanced technological method was reported to have been applied in investigating AB_5 type hydride electrode alloys [1–4]. The chief advantage of rapidly solidified AB_5 type hydride electrode alloys is that their electrochemical cyclic endurance can be improved greatly while the discharge capacity remains almost the same [2]. A few papers have reported on the application of rapid solidification technique to the AB_2 type Zr-based Laves phase alloys [5,6]. However, many important problems such as the phase formation mechanism, phase abundance and microstructure, electrochemical characteristics etc. have not been studied deeply enough. The relationship between the rapid solidification process parameters and electrochemical properties of the alloys has not been considered.

For the aforesaid reasons, we choose $Zr(Ni_{0.55}V_{0.1}Mn_{0.3}Cr_{0.55})_{2.1}$ alloy as the electrode alloy and studied the relationship among different cooling rates and microstructure, crystal structure as well as electrochemical properties of the alloy systematically. The results indicate that crystal structure, microstructure, phase abundance and electrochemical properties of the alloy change to different extents with the cooling rate of the rapid solidification process.

2. Experimental

All the melt spun alloys used in this study had same composition with different cooling rate. The master alloy was prepared by arc melting under an argon atmosphere,

*Corresponding author.

0925-8388/99/$ – see front matter
PII: S0925-8388(99)00458-2

Table 1
Relationship between cooling rate and thickness of melt spun ribbons

Thickness (μm)	105	59	35	30
Cooling rate (10^6 K s^{-1})	0.435	1.38	3.92	5.33

and re-melting several times to ensure the uniformity. The ribbons were produced by a melt-spinning machine with a single copper roller under an argon atmosphere. The cooling rate was estimated by the following formula [7]

$$R = Ad^{-2}$$

where R is the cooling rate ($K\,s^{-1}$), d is the ribbon thickness (μm), A is a constant, which is determined to be 4.8×10^{-3} ($m^2\,K\,s^{-1}$) according to our experiment. The cooling rates of the ribbon of different thickness are shown in Table 1.

Samples of melt spun alloys were pulverized mechanically in the air. The data of powder X-ray diffraction were tested in Rigaku D/max-3B diffractometer using CuKα radiation and analyzed with Rietveld method. More detail information about the XRD experiment is reported in another paper [8]. The microstructure was observed with transmission electron microscope (TEM).

The part of alloy powder that passed through 320 mesh sieve was used for preparation of the electrodes. The alloy powder was mixed with fine copper powder in a weight ratio of 1:2 and pressed into pellets of 10 mm diameter. Every pellet contains some 100 mg of hydrogen storage alloy powder. Each pellet was put into a copper cylindrical holder to form an electrode which was charged and discharged in a 6 M KOH electrolyte in a standard trielectrode electrolysis cell opened to the atmosphere. A nickel plate was used as the counter electrode and Hg–HgO–OH^- used as reference electrode. The discharge cut-off potential was −0.6 V with respect to the Hg–HgO–OH^- reference electrode. The electrodes were fully charged at 100 mA g^{-1} and discharged at 50 mA g^{-1}.

3. Results

3.1. XRD analysis

Fig. 1 shows the XRD stacking patterns for all the rapidly solidified alloys. Fig. 2 is one of the Rietveld analysis pattern for the alloy with a cooling rate of 5.33×10^6 K s^{-1}. All the peak positions of C14 and C15 phased are shown in Fig. 2. The upper line designates as C15 Laves phase and the lower C14 Laves phase. The patterns of rapidly solidified alloys contain two kinds profile. One is dispersive microcrystalline profile, another is sharp peaks belonging to C15 Laves phase. There is neither non-Laves nor amorphous phase in melt-spun alloy. This differs from the report of Fujinara et al. which contains Zr_7Ni_{10} non-Laves phase [6]. Table 2 lists the numerical result of fitting criteria for all examples. The value of fitting index is in the scope of general Rietvald analysis [9]. These results indicate the model and results are reliable. Tables 3 and 4 summarize the XRD data analyzed by Rietveld method. In Table 4 M_{nn} (or M_{33}) designates the crystalline dimension in a (or c) directions. ϵ_{nn} (or ϵ_{33}) designates the strain in a (or c) directions. It shows that the strains in all directions are very small.

The data in Table 3 indicates that C15 and/or C14 Laves phase abundance of rapidly solidified alloys varies

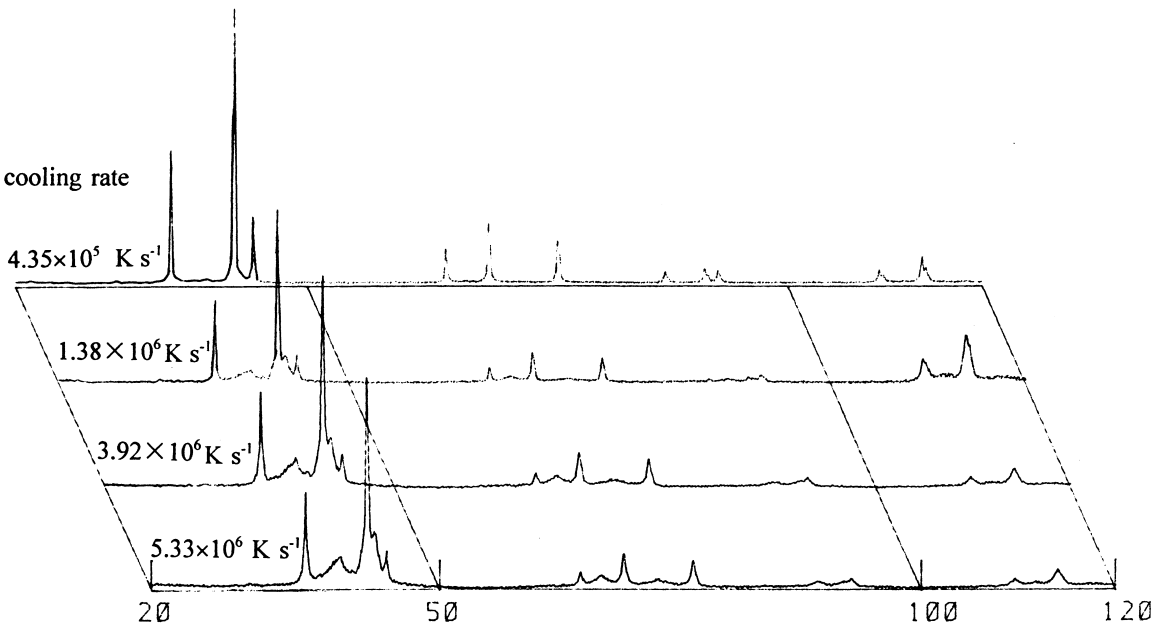

Fig. 1. XRD stacking patterns for rapidly solidified alloys at different cooling rates.

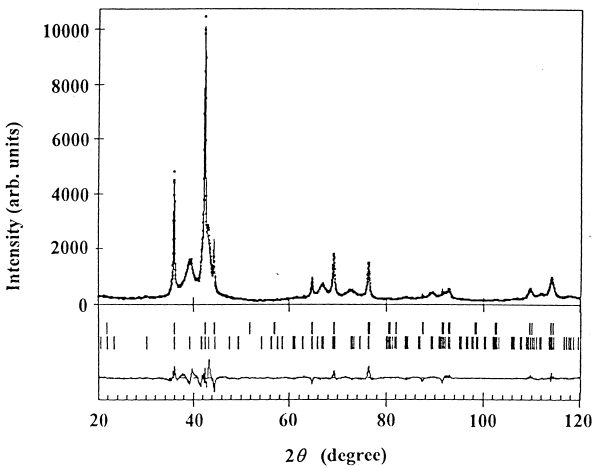

Fig. 2. Observing (dots), calculated (line) and difference Cu Kα X-ray powder diffraction pattern for C14, C15 Laves Phase at cooling rate 5.33×10^{6} K s^{-1}.

Table 2
Fitting index of Rietveld analysis for rapidly solidified alloys[a]

Cooling rate (K s^{-1})	R_{wp}	R_p	S	R_B	
				C14	C15
4.35×10^{5}	5.47	4.21	1.60	6.23	3.17
1.38×10^{6}	7.49	5.76	1.81	6.69	3.79
3.92×10^{6}	12.59	9.76	2.52	4.06	8.15
5.33×10^{6}	11.33	8.67	2.37	3.19	7.54

[a] R_{wp}, weighted pattern factor; R_p, pattern factor; R_B, Bragg factor; S, Goodness of fit.

with the change of cooling rate. When cooling rate reaches 4.35×10^{5} K s^{-1}, the main phase of the rapidly solidified alloy is C15 Laves phase. It contains 88.3 wt.% C15 phase and 11.7 wt.% C14 Laves phase. With the increase of cooling rate, the abundance of C15 Laves phase decreases and the C14 Laves phase increases. When the cooling rate reaches 5.33×10^{6} K s^{-1}, C15 phase become less than C14 Laves phases, with 43.6 wt.% C15 Laves phase constitutes and 56.4 wt.% C14 Laves phase.

3.2. Microstructure

Fig. 3 is the microstructure of rapidly solidified alloy with cooling rate 3.92×10^{6} K s^{-1}. Fig. 3a is the morphological appearance of microcrystalline C14 Laves phase. Fig. 3b is the fine grain C15 Laves phase. Through analyzing the XRD data and TEM observation (see Table 4 and Fig. 3), we discover a new microstructure of C14 Laves phase, the microcrystalline C14 Laves phase. Its morphological appearance is a lamellar structure with the distance between layers equaling about 30 nm. Every layer is composed of lots of minute crystallites with dimensions about 3.5 nm in the *a* (or *b*) direction and about 1 nm in the *c* direction (see Table 4). We also discover that C15 Laves phase assumes extremely fine granular morphology. Each fine grain is again composed of lots of minute crystallites. The result in Table 4 indicates that the crystallite of microcrystalline C14 Laves phase has almost the same size at different cooling rates, but the size of crystallite in C15 Laves phase is comparatively bigger in size and becomes finer as the cooling rate increases.

In addition, Table 3 also shows that there are a small changes in cell parameters. The cell volume of C15 increases and the cell volume of C14 decreases as the cooling rate decreases, also all the alloys have the same composition.

Table 3
Phase abundance and cell parameters for rapidly solidified alloys

Cooling rate (K s^{-1})	Abundance (wt.%)		Cell parameters (nm)		
	C14	C15	C15	C14	
			a	*a*	*c*
4.35×10^{5}	11.73(2.1)	88.29(1.8)	0.70591(1)	0.5004(2)	0.8096(7)
1.38×10^{6}	49.94(2.52)	51.06(2.42)	0.70446(2)	0.5021(7)	0.8100(3)
3.92×10^{6}	54.64(1.90)	45.33(1.79)	0.70513(2)	0.4995(4)	0.8120(2)
5.33×10^{6}	56.37(1.98)	43.63(1.76)	0.70535(2)	0.5003(5)	0.8133(2)

Table 4
Mean crystalline size and micro-strain for rapidly solidified alloys[a]

Cooling rate K s^{-1}	C15		C14			
	M_{nn} (nm)	$\langle\epsilon^2\rangle_{nn}^{1/2}$	M_{nn} (nm)	$\langle\epsilon^2\rangle_{nn}^{1/2}$	M_{33} (nm)	$\langle\epsilon^2\rangle_{33}^{1/2}$
4.35×10^{5}	54.1(4)	0.0003(1)	3.3(5)	0.00001	1.02(8)	0.0035
1.38×10^{6}	31.6(10)	0.0012(2)	3.0(1)	0.00001	0.99(2)	0.0025
3.92×10^{6}	24.2(5)	0.0013(3)	3.7(2)	0.00001	1.18(2)	0.0030
5.33×10^{6}	17.8(5)	0.0014(2)	3.6(2)	0.00001	1.02(2)	0.0024

[a] $nn=11=22=33$ for C15, along *a*, *b*, *c* axis direction; $nn=11=22$ for C14, along *a*, *b* axis direction, 33 along *c* axis direction.

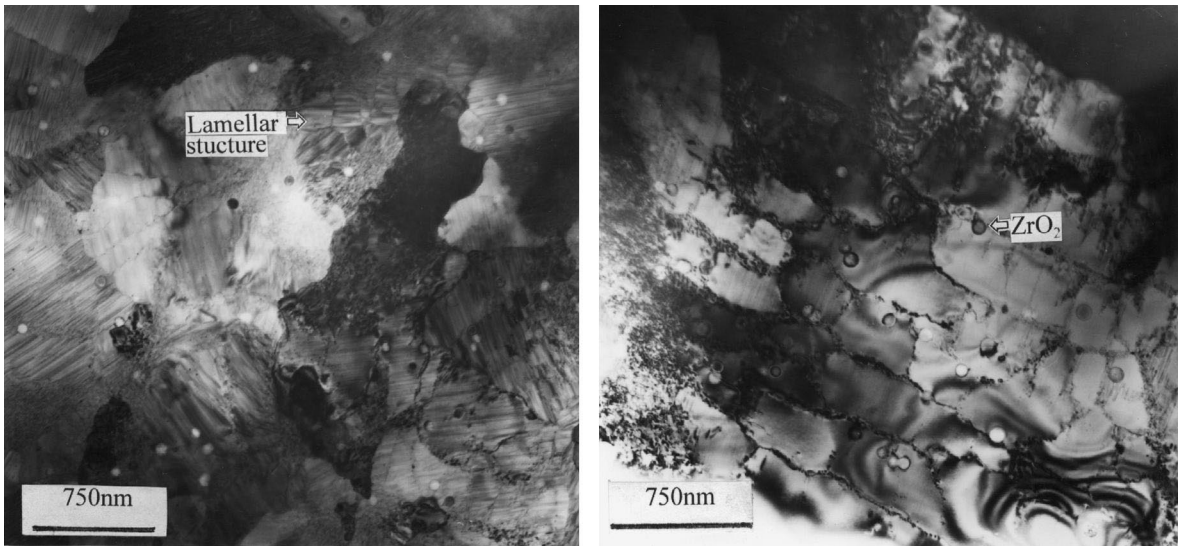

Fig. 3. Microstructure of rapidly solidified alloy at cooling rate 3.92×10^6 K s^{-1} (a) Microcrystalline C14 Laves phase with lamellar structure (b) fine grain C15 Laves phase, the cross-section of the columnar structure.

3.3. Electrochemical properties

Fig. 4 shows the effect of cooling rate on the activation property of the alloy. The alloy become more difficult to activate as the cooling rate in the melt-spinning alloy increases. At cooling rates 4.35×10^5, 1.38×10^6, 3.92×10^6 and 5.33×10^6 K s^{-1}, the activation cycles required are 12, 20, 25 and 55, respectively. From the viewpoint of practical application, the cooling rate of melt-spinning alloy $Zr(Ni_{0.55}V_{0.1}Mn_{0.3}Cr_{0.55})_{2.1}$ should be chosen a little lower, such as around 10^5 K s^{-1}.

Fig. 5 shows the relationship between C14 Laves phase abundance and activation cycles for melt spinning alloy $Zr(Ni_{0.55}V_{0.1}Mn_{0.3}Cr_{0.55})_{2.1}$. Activation cycles required are in direct proposition to the quantity of C14 Laves phase in the range of 11.7–54.67 wt.% phase abundance. Fig. 6 indicates the effect of the phase abundance of microcrystalline C14 Laves phase or/and C15 Laves phase on the discharge capacity of rapidly solidified alloys. With the increase of C14 Laves phase or decrease of C15 Laves phase, the discharge capacity of rapidly solidified alloys reduces.

Fig. 7 shows the cycle life of the rapidly solidified alloy at different cooling rates. The cycle lives of the melt-spinning alloys are all very long at whatever cooling rates, and with the increase of cooling rate, the cycle life shows the tendency of prolongation. After 500 charging–discharging cycles, the residual capacity is higher than 78.6% of the initial capacity. It also increases with the cooling rate. Fig. 8 is the relation between the amount of Laves

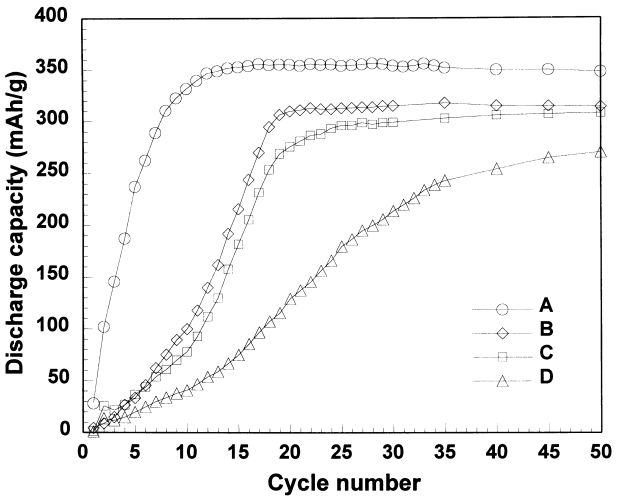

Fig. 4. Activation curves of rapidly solidified alloys at different cooling rate. The cooling rate are (A) 4.35×10^5 K s^{-1} (B) 1.38×10^6 K s^{-1} (C) 3.92×10^6 K s^{-1} (D) 5.33×10^6 K s^{-1}.

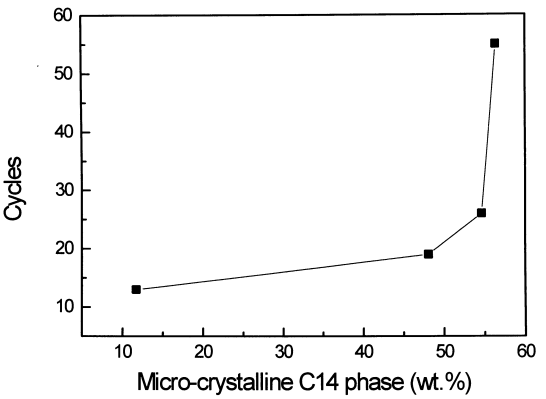

Fig. 5. Relationship between activation cycles to reach maximum capacity and relative amount of the microcrystalline C14 Laves phase.

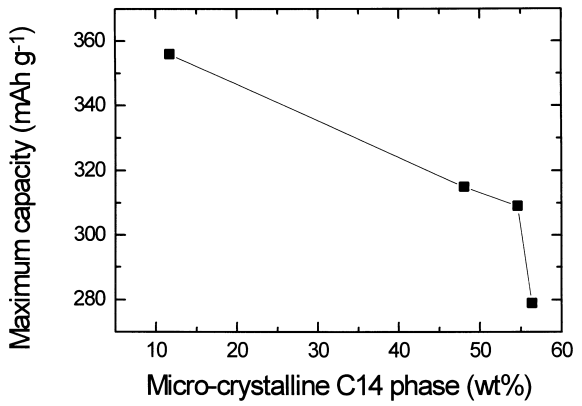

Fig. 6. Relationship between maximum capacity and relative amount of the microcrystalline C14 Laves phase.

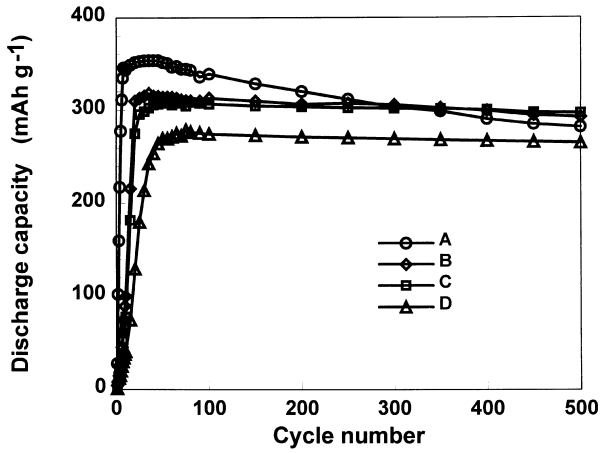

Fig. 7. Cycle life of rapidly solidified alloys at different cooling rate.The cooling rate are (A) 4.35×10^{5} K s^{-1} (B) 1.38×10^{6} K s^{-1} (C) 3.92×10^{6} K s^{-1} (D) 5.33×10^{6} K s^{-1}.

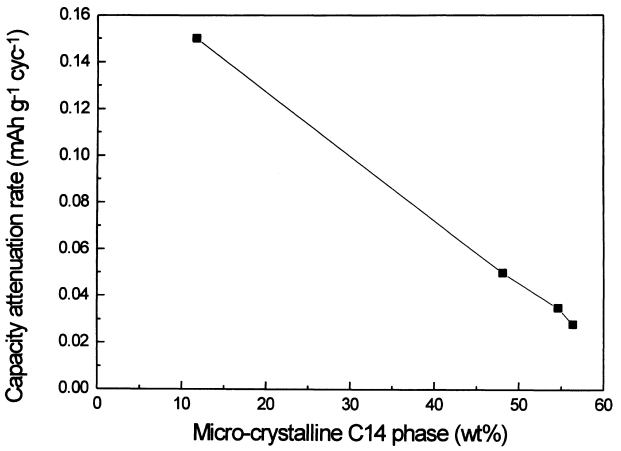

Fig. 8. Effect of microcrystalline C14 Laves phase on mean capacity attenuation rate $\eta, \eta = \Delta C/\Delta n$, $\Delta C = C_{max} - C_{500}$, $\Delta n = N_{max} - N_{500.}$

phase and mean attenuation rate of cycle life. It is shown in Fig. 8 that microcrystalline C14 Laves phase is beneficial for maintaining the capacity after long charging–discharging cycles.

4. Discussion

There is an obvious difference between block C14 Laves phase in conventional cast alloys and the morphologically lamellar microcrystalline C14 Laves phase that we discovered in the rapidly solidified alloys. The formation of microcrystalline C14 Laves phase is closely related to the cooling rate of the alloy in rapid solidification process. The microcrystalline C14 Laves phase increases in amount with the cooling rate. There must be a critical cooling rate for Zr-base AB_2 type Laves phase alloy, above which microcrystalline C14 Laves phase would appear and at higher cooling rates, more microcrystalline C14 Laves phase appear.

The electrochemical properties of rapidly solidified alloy are affected by cooling rates, but actually they are determined by the abundance of microcrystalline C14 Laves phase. As the microcrystalline C14 Laves phase increases (or C15 Laves phase decreases), the activation cycles of rapidly solidified alloy increases, the discharge capacity reduces and its cycle life prolongs. Particularly, when the microcrystalline C14 Laves phase increases to above 55 wt.%, the activation cycles increases abruptly and discharge capacity reduces sharply (see Figs. 5 and 6).

According to composition, C14 and C15 Laves phase ought to have the same electrochemical properties, yet they are quite different. The difference, we believe, is due to the variation in thermodynamic and/or kinetic characteristics. Activation is the most important factor that affects all other electrochemical properties. The capacity would be zero if the alloy is not activated. The microcrystalline C14 Laves phase is the component that is activated very slowly. Both Figs. 4 and 5 reveal this property. The big difference in discharge capacity of rapidly solidified alloys with different cooling rates is due to the different content of microcrystalline C14 Laves phase. We have found through experiment that when microcrystalline C14 Laves phase was treated with hot alkaline, its discharge capacity became higher. The mechanism of this effect is not very clear, but it may be partly due to improved surface activation. There are a lot of things not yet clear about the effect of microcrystalline C14 Laves phase on the electrochemical properties of the rapidly solidified alloys. Further investigation is needed.

5. Conclusions

(1) Lattice parameter, cell volume and phase abundance of $Zr(Ni_{0.55}V_{0.1}Mn_{0.3}Cr_{0.55})_{2.1}$ all change with the cooling

rate. As the cooling rate increases, the cell volume of C15 phase increases and C15 phase abundance decreases. On the contrary, cell volume of C14 phase decreases and the abundance of C14 phase increases. The change of cell parameters and phase abundance with the cooling rate is the main reason for the changes in electrochemical properties.

(2) A new microstructure–microcrystalline C14 Laves phase is identified in rapidly solidified alloys. The microcrystalline C14 Laves phase is of lamellar morphology. Every layer is composed of a lots of minute crystallite with about 3.5 nm in *a* (or *b*) direction and about 1 nm in *c* direction. The electrochemical properties of rapidly solidified alloy are closely related with this new microstructure.

(3) The electrochemical properties of rapidly solidified alloys are closely related to the abundance of the microcrystalline C14 Laves phase which is tied closely with its cooling rate. The change of the phase abundance is the main reason for the changes of electrochemical properties.

Acknowledgements

This work is supported by National Advanced Materials Committee and National Natural Science Foundation of China (No. 59601006, 59671016).

References

[1] R. Mishima, H. Miyamura, T. Sakai, N. Kuriyama, H. Ishikawa, I. Uehara, J. Alloys Compd. 192 (1993) 176–178.
[2] T. Weizhong, S. Guanfei, J. Alloys Compd. 203 (1994) 195–198.
[3] Y. Nakamura, H. Nakamura, S. Fujitani, I. Yonezu, J. Alloys Compd. 210 (1994) 299–303.
[4] N. Higashiyama, Y. Matsuura, H. Nakamura, M. Kimoto, M. Nogami, I. Yonezu, K. Nishio, J. Alloys Compd. 253–254 (1997) 648–651.
[5] M. Ciureanu, J.O. Sstrom-Olsen, D.H. Ryan, P. Rudkowski, G. Rudkowska, B. Bondoc, J. Electrochem. Soc. 141 (12) (1994) 3291–3295.
[6] S. Fujiwara, B. Kurishinann, Y. Muriwaki, I. Matsumoto, Electrochem. Soc. Proc. 94–27 (1994) 172–183.
[7] H. Jones, Rep. Prog. Phys. 36 (1973) 1425–1497.
[8] G. Lu, K. Shu, L. Chen, X. Song, X. Yang, Y. Lei, Q. Wang, in: International Symposium on Metal–Hydrogen Systems (abstract), Fundamentals and Applications, Oct. 4–9 (1998), Hangzhou, China, 1998.
[9] Edward Prince, in: R.A. Young (Ed.), The Rietveld Method, Oxford University Press, Oxford, 1993.